Numerical Methods in Civil Engineering, 6-3 (2022) 37-50

Numerical Methods in Civil Engineering

Journal Homepage: https://nmce.kntu.ac.ir/

Evaluating of Relative and Absolute Cumulative Input Energy Time History subjected to Forward Directivity Earthquakes

Navid Siahpolo[*], Seyed Abdonnabi Razavi[**], Hamid Beiraghi[***]

ARTICLE INFO

RESEARCH PAPER

Article history:
Received:
June 2021.
Revised:
September 2021.
Accepted:
November 2021.

Keywords:
Input Energy
Steel Moment Frame
Near-fault Earthquake
Absolute Energy
Relative Energy.

Abstract:

In this article, to study the effect of pulse-type near-fault earthquakes on the seismic demands of steel moment frames, 15-story 2D-frame was analyzed under the influence of 20 near-fields with forward directivity effect and 2 far-field records. The relationship between effective cyclic energy, and displacement demands, velocity and hysteretic curve of single degree of freedom systems in two near- and far-fault earthquakes were evaluated. Then, by examining the relative and absolute cumulative input energy history along with the kinetic energy in one section and the maximum inter-story drift for 4 different levels of nonlinear behaviour (R = 1.0, 2.0, 4.0, and 6.0) in a section, the effect of higher modes was evaluated. The study of inter-story drift profile for two near-fault earthquakes with and without visible pulse indicated the formation of maximum drift concentration, IDR_{max}, in the upper stories for low nonlinear degrees in record with visible pulse, which itself is an indication of its effect on higher mode contribution. However, in the pulse-free records, in addition to IDR_{max} intensification in the upper stories, the lower stories also have large structural demands. In other words, in these records, in the lower stories, dynamic instability is mainly involved.

1. Introduction

In the vicinity of active faults, the ground motion is powerfully affected by fracture mechanism and direction of fault rupture with respect to site (for example fling-step and forward directivity motion effects), and persistent static deformation at fault known as fling steps motion. Therefore, near-fault earthquake parameters cause a considerable amount of fault failure energy to appear in the form of a pulse excitation with long periods (it should be noted that the backward directivity effects lack the pulse nature). The ground motion with such pulse-type is often seen at the beginning of velocity time history and tends to extend the long period of the acceleration response spectrum. (1994), Kobe (1995), Kochi (1999), Davies and Chi-Chi Taiwan.

* *Corresponding author: Department of Civil Engineering, Institute for Higher Education ACECR, Khouzestan, Iran. Email: siahpolo@acecr.ac.ir*
** *Department of Civil Engineering, Abadan Branch, Islamic Azad University, Abadan, Iran.*
*** *Department of Civil Engineering, Mahdishahr Branch, Islamic Azad University, Mahdishahr, Iran.*

In this case, the structure dissipates a significant amount of earthquake energy with a minor number of disturbances over a large range and imposes significant structural demands. As a result, the risk of brittle failure in structural elements is reinforced by poor execution details. The determinant effects of such a phenomenon were observed during the earthquakes of Arzakan (1992), Landers (1992), and Northridge.

Since the mid-1950s, when Housner (1956) introduced and proposed the limit design method to provide energy dissipation capacity of structural elements firstly [1], energy-based design methods have been re-considered by researchers. In this regard, a considerable number of research papers have been written and presented with a design approach based on energy concepts [2-5]. It should be noted that the most prominent study that led to the concept of input and output energy re-considered as a criterion for measuring structural damage, is a paper written by Uang and Bertero (1990) [6]. This study proved the significance of absolute input energy and showed that

in the time history of input energy there is always a significant jump in energy. Subsequently, a considerable number of studies were conducted to obtain an appropriate estimate of the energy demands and the mechanism of its loss in the structure. One of the achievements is the introduction of energy-based spectra [7-10]. In addition, in other studies, systematization of the controlled input energy process has also been developed in seismic design and its control methods [11-12]. Kalkan and Kunnath (2006) studied the non-elastic seismic behavior of steel structures used in SAC project. For this purpose, three steel structures were modeled and analyzed as 2D frames with 3, 9 and 12 stories by OpenSEES software. On the one hand, the properties of forward directivity bring more demands rather than fling-step. This is justified by the presence of forward and backward moment of the earthquake with directivity in the early and late phase of the pulse. In forward directivity effect, the demand for upper stories is almost twice than fling-step. The effect of higher modes was not seen in fling-step, but for Tp/T less than 0.8 seconds, this effect is quite evident for forward directivity [13]. In a study by Kamali-Firozabadi (2011), the use of energy method was investigated to evaluate the displacement demand of steel moment frames. He suggested a method, based on the concept of velocity, to more accurately estimate the record's transient energy [14]. Applying the concept of earthquake input energy was examined in a study by Vahdani et al. (2017). Using nonlinear dynamic analysis for 4 damping ratios and 4 ductility values, caused relative input energy spectra per unit mass for 4 earthquakes in Iran. The study shows that the effect of ductility values on the relative input energy spectrum is more noticeable than the effect of damping ratio [15].

In general, the main objective of this paper is to examine the definition of input energy using the latest results related to near-fault earthquakes. Given the access to a significant number of near-fault earthquakes at present, this paper specifically examines the effect of forward directivity effects on energy entering the structure. The evaluation approach here is the concept of the behaviour coefficient of an equivalent SDOF system (R value). It should be noted that near-fault earthquakes are often classified into two forms, forward directivity effects and fling-step motion. A prominent feature of forward directivity effect is the presence of a significant pulse in the velocity record and sometimes in the earthquake acceleration. Recent studies on near-fault earthquakes indicate that for seismic design of structures, in addition to the effects of frequency content evident in the earthquake acceleration history, special consideration should be paid to the dominant pulse of velocity time history. For example, Cheng Fang et al. (2018) investigated the maximum story acceleration and residual inter-story drift of steel moment and braced frames under near-fault earthquakes with forward directivity motion. They proved that the structural responses were highly dependent on spectral acceleration, PGV/PGA ratio, and record pulse period [16]. Likewise, a study by Lifeng Xin et al. (2019) conducted on concrete filled steel tube (CFST) long opening bridges showed that fling step movement incorporates static and dynamic pulses, both of which have significant effects on seismic responses [17]. Although the record pulse effect has been considered in various studies, the importance of local pulses in acceleration of near fault earthquakes and their effect on the intensity of damages was first proposed by Bertero (1976) [18].

Accordingly, in this study, the inelastic demands in terms of energy were first calculated for a SDOF system with different period, then a 15-stories 3-bay 2D steel moment frame used under the influence of 20 near-fault earthquakes with forward-directivity effects, as well as two far-fault records, for evaluation and comparison. On the basis of Fig. 3, the models have been analyzed under all of the aforementioned earthquakes; however, to summarize and avoid lengthening the paper and, of course, a more detailed discussion, merely the results of a number of records are presented. Also, the response of 15-stories structure for different values of R has been investigated. This issue has been investigated by evaluating various parameters which are discussed below. What distinguishes this study from previous studies is that none of the previous studies has explicitly considered the concept of the effect of earthquakes (The existence of distinct pulses in the acceleration history of near-fault earthquake) on defining absolute and relative input energy. In addition to evaluating the properties of near-fault earthquakes such as acceleration pulses and vicinity of pulse period with structural vibration period, the effect of degree of nonlinearity on damage distribution and relative and absolute input energy distribution have been considered. In addition, what is calculated for SDOF system is the response spectrum of the input energy in the inelastic domain, which has been actually considered less by previous studies on near-fault earthquakes.

2. Research Method

2.1 Basic formulation in SDOF system input energy

The structure dynamics principles include the motion equation of damping SDOF system as follows:

$$m\ddot{u}_t + c\dot{u} + f(u) = m\ddot{u}_t + c\dot{u} + f(u) = 0 \quad (1)$$

In this equation, m is the structure mass, c is the coefficient of damping, f(u) is the spring force stored in the linear system, u_t is the absolute displacement, u_g is the displacement of the ground, and u is the relative

displacement of the system to the earth. Eq. (1) can be rewritten as Eq. (2):

$$m\ddot{u} + c\dot{u} + f(u) = -m\ddot{u}_g m\ddot{u} + c\dot{u} + f(u) = -m\ddot{u}_g \quad (2)$$

By integrating equations (1) and (2) to the relative displacement, u, two classifications of the input energy are obtained. If Eq. (1) is integrated to u, the absolute energy formulation of SDOF system with viscous damping results from a horizontal earthquake:

$$m\frac{(\dot{u}+\dot{u}_g)}{2} + \int(c\dot{u})du + \int f(u)du = \int m(\ddot{u}_g + \ddot{u})\,du_g = \int m(\ddot{u}_g + \ddot{u})\,\ddot{u}_g dtm\frac{(\dot{u}+\dot{u}_g)}{2} + \int(c\dot{u})du + \int f(u)du = \int m(\ddot{u}_g + \ddot{u})\,du_g = \int m(\ddot{u}_g + \ddot{u})\,\ddot{u}_g dt \quad (3)$$

Equation (3) can be re-written in the general form of Eq. 4. In this case, all types of energy components can be defined:

$$E_K + E_\xi + E_s + E_H = E_{AI} \quad (4)$$

where E_{AI} is absolute input energy, E_K is absolute kinetic energy, E_ξ is damping energy, E_s is elastic strain energy, and E_H is plastic strain energy (irreversible cyclic energy). On the one hand, if Eq. (2) is integrated to u, Eq. (5) is obtained to introduce the relative energy of SDOF system:

$$m\frac{\dot{u}}{2} + \int(c\dot{u})du + \int f(u)du = -\int m(\ddot{u}_g)\,du = -\int m\ddot{u}_g\,\dot{u}dt \quad (5)$$

The closed form of energy components in Eq. (5) can be written as Eq. (6):

$$E_{KR} + E_\xi + E_s + E_H = E_{RI} \quad (6)$$

where E_{RI} is relative input energy, E_{KR} is relative kinetic energy, E_I denotes the work that affects the structure by the inertia force ($m\ddot{u}_t$), which is equivalent to the work done by the total base shear force due to ground motion. On the other hand, E_{RI} is the same to the work done by a fixed-base structure with equivalent lateral force. As a result, this energy has no effect on rigid body motion. The distinction between the two energies is in fact the difference in absolute and relative kinetic energies, because in both equations (4) and (6) the values of the damping, elastic strain and plastic energy are the same. The difference in the two energy classifications can be written as Eq. (7):

$$E_{AI} - E_{RI} = E_K - E_{KR} = \frac{1}{2}m\dot{u}_g^2 + m\dot{u}_g\dot{u} \quad (7)$$

The right side of equation (7) has two expressions. The first expression is kinetic energy due to the velocity of the ground, and the second one is the work done by the ground acceleration in terms of the gradual increase in the displacement of the structure. In an initial conclusion, it can argued that the size of the relative and absolute input energy will vary for very hard and very soft structures. In flexible (soft) structures whose vibrational period is much longer than the dominant period of the ground motion, the structure mass remains at its original position while the base of the structure is displaced simultaneously and as much as the ground motion. In this case, the absolute input energy to the structure is zero while the relative energy is transferred to the structure. In contrast, for hard structures, the relative displacement of the mass due to the ground motion is negligible, resulting in the relative energy of earthquake input which is near zero and a noteworthy amount of absolute energy which is practical to the structure.

2.2 SDOF and MDOF model description

The basic research model, hereinafter referred to as FRN15B3, has 15 stories and 3 bays. The height of all stories is constant and 4 m and the length of the spans is 5 m. The two-dimensional steel moment frames used in this study was selected as a sway-special. All the aforementioned frames have been subjected to gravity and seismic loading. In gravity loading, the dead load, the equivalent partitioning load and the live load of the stories were selected as 550, 200 and 250 kg/m² respectively. Dead load plus 20% of live load is assumed as seismic story mass. Construction site soil is type III in high seismic risk zone. Moreover, the models have residential occupancy [19]. The model is designed using Etabs2016 [20] under pseudo-dynamic analysis and basic design shear matching using LRFD method [21]. Some assumptions such as rigid full-strength beam column connections, rigid full-strength column bases, and a horizontal diaphragm restraint for the nodes of each floor to account for the in-plane rigidity of the composite slab has been considered in ETABS models. In addition, to the strength-based design, the stiffness distribution of the frames in height has been adjusted so that the maximum inter-story drift angle is limited to the permissible values set in Standard 2800 4th edition. The plate girder section was used for the beams and the BOX section was used for the columns. The seismic compact cross section criteria were observed in all sections. The geometry profile and side view of FRN15B3 frame is shown in Tables 1-3 and Figure 1.

Table 1: Beam and Column Sections

Stories	FRN15B3	
	Column	Beam
1~3	C4	B2
4~6	C3	B2
7~8	C2	B2
9~11	C2	B1
12~15	C1	B1

Table 2: The column sections

Model	Section types	b_f	t_f	h_w	t_w
BOX 300X25	C1	300	25	300	25
BOX 350X30	C2	350	25	350	25
BOX 400X30	C3	400	30	400	30
BOX 450X30	C4	450	30	450	30

Table 3: The beam sections

Model	Section type	b_f	t_f	h_w	t_w
TW500F250TH15	B1	250	20	500	20
TW550F250TH20	B2	250	20	550	20

For a better interpretation of the results, the main vibrational properties of this building system are presented in Table 4.

Table 4: Dynamic Profile of FRN15B3

	1st Mode	2nd Mode	3rd Mode	4th Mode	5th Mode
T_i(sec)	2.45	0.89	0.51	0.36	0.35
PF_i	1.39	-0.58	0.31	-0.23	0.17
W_i/W (%)	74.08	13.32	4.44	2.36	1.41

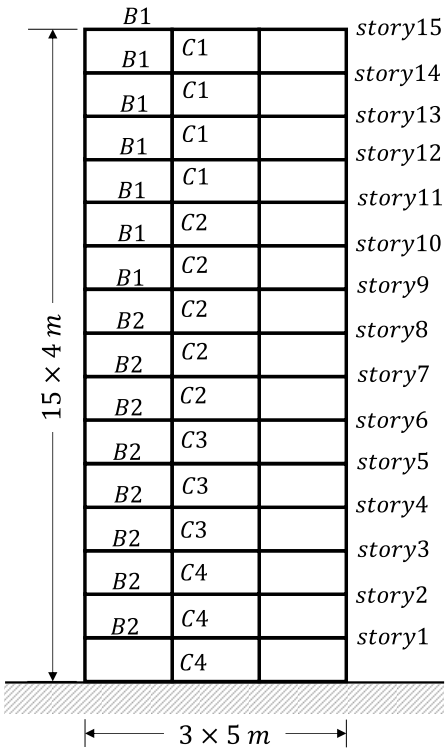

Fig. 1: Side view of FRN15B3 frame

2.3 Models for Nonlinear Dynamic Analysis

The OpenSEES software [22] is utilized to simulate nonlinear models for the steel MRFs. Beams are modelled as displacement-based elements with fiber-section properties. Each fiber is assumed to reveal uniaxial bilinear elasto-plastic stress-strain cyclic behaviour. Panel zones are reflected rigid and elastic. Force-based fiber elements are used to model the columns to capture moment-axial force interaction effects accurately. Additionally, to the assumption of the axial rigidity of the composite slab, a rigid diaphragm constraint is enacted at the nodes of each floor, while to account for the P-Δ effects of the gravity loads stand-in of the tributary plan area of the steel MRF, the Corotational Coordinate Transformation is involved in the models. To integrate the motion equations of the steel MRFs subjected to earthquake ground motion, the Newmark method is used with constant acceleration. To minimalize the unbalanced forces within each integration time step, the Newton method with tangent stiffness is used, while an automatic technique of decreasing the time step was engaged to overcome convergence issues. The natural 5% damping ratio at the first two modes of vibration is modelled by using a Rayleigh damping matrix that excludes from its stiffness proportional component all the nonlinear springs with high initial stiffness, so that large damping forces can escape. A nonlinear force-controlled static analysis is first accomplished under the gravity loads of the seismic design combination and then nonlinear dynamic analysis is accompanied.

2.4 Earthquake specifications

In a classification, near-fault records can be distinguished from far-fault earthquakes based on engineering judgments. Especially if the earthquake velocity time history is available, it is much easier to detect. Another criterion of distinguishing near-fault earthquake is the source to site distance. Usually, in near-fault earthquakes, the distance between 15 and 30 km is defined as the near-fault distance. According to studies conducted by Baker [23], a general definition is presented for detecting near-fault earthquakes. According to this definition, three features should be considered simultaneously to be assigned to a near-fault earthquake [23]. These criteria are as follows:

- Pulse index greater than 0.85
- Pulse formation at the early moments of velocity time history
- PGV of earthquake exceeding 30 m/s

Table 5: 20 near fault records, with forward-directivity effect, perpendicular to fault component (NF-SN)

Record No.	Earthquake Name	Year	Station Name	PGA [a] (g)	Mw [b]	R [c] (km)	T_P [d] (S)
SN1	Imperial Valley-06	1979	El Centro Array #4	0.61	6.53	7.05	4.61
SN2	Northridge-01	1994	Newhall - Fire Sta	0.18	6.69	5.92	1.03
SN3	Northridge-01	1994	Newhall - W Pico Canyon Rd.	0.33	6.69	5.48	2.40
SN4	Northridge-01	1994	Rinaldi Receiving Sta	0.08	6.69	6.50	1.23
SN5	Northridge-01	1994	Sylmar - Converter Sta East	0.58	6.69	5.19	3.52
SN6	Kobe, Japan	1995	KJMA	1.05	6.90	0.96	0.95
SN7	Kobe, Japan	1995	Takarazuka	0.94	6.90	0.27	1.42
SN8	Landers	1992	Yermo Fire Station	0.10	7.28	23.62	7.50
SN9	Imperial Valley-06	1979	El Centro Array #6	0.65	6.53	1.35	3.83
SN10	Northridge-01	1994	Jensen Filter Plant	0.12	6.69	5.43	3.52
SN11	Imperial Valley-06	1979	EC County Center FF	0.32	6.53	7.31	4.51
SN12	Imperial Valley-06	1979	EC Meloland Overpass FF	0.44	6.53	0.07	3.34
SN13	Morgan Hill	1984	Coyote Lake Dam (SW Abut)	0.23	6.19	0.53	0.95
SN14	Loma Prieta	1989	Gilroy - Gavilan Coll.	0.25	6.93	9.96	1.79
SN15	Loma Prieta	1989	LGPC	0.84	6.93	3.88	4.39
SN16	Northridge	1994	Westmoreland	0.40	6.70	29.00	0.30
SN17	Northridge-01	1994	Jensen Filter Plant Generator	0.12	6.69	5.43	3.52
SN18	Northridge-01	1994	Sylmar - Converter Sta	0.65	6.69	5.35	3.47
SN19	Northridge-01	1994	Sylmar - Olive View Med FF	0.45	6.69	5.30	3.10
SN20	Kocaeli, Turkey	1999	Gebze	0.30	7.51	10.92	5.78

[a] Peak Ground Acceleration, [b]Moment Magnitude, [c] Closest distance from the recording site to the ruptured area , [d] Predominant Period, (Kramer,1996) [24]

Table 6: 2 Far-fault records (FF-OR)

Record No.	Earthquake Name	Year	Station Name	PGA[a] (g)	Mw[b]	R[c] (km)	T_P[d] (S)
OR2	Imperial Valley	1992	ElCentro Array #6	0.32	6.95	44.60	0.56
OR9	Tabas	1978	Ferdows	0.10	7.35	91.14	0.24

[a] Peak Ground Acceleration, [b]Moment Magnitude, [c] Closest distance from the recording site to the ruptured area , [d] Predominant Period, (Kramer,1996) [24]

According to the explanations provided, in this paper, 20 strike-normal records with forward directivity effect were selected. NF-SN has been designated for identification and brevity. The features of these records are presented in Table 5. Meanwhile, two far-fault earthquake records have also been selected to compare the results of near-fault pulse and far-fault earthquakes. Table 6 shows an overview of selected far-fault earthquakes and their acceleration history. In this paper, far-fault earthquakes are named FF-OR. The models have been analyzed for all the records mentioned, however, for brevity and discussion, the results of just a few are presented in Table 5.

3. Verification

In numerical studies, and particularly when there is a demand for preparing a database, the uncertainty of the accuracy of the developed model can lead to incorrect results. In order to escape such an event in this study, all models are validated based on the model shown in Figure 2. The building was designed by Phase 2 of SAC project by consulting engineers Brandow and Johnson. The dimensions of this building are 45.73 in 45.73 meters and its height is 37.19 meters. The stories height was 3.96 meters and frames consisted of five equal 9.15 meters' bay. The frames around the structure are of the steel moment that play the role of the lateral bearing system. All connections are pinned at mid bays and continuous at lateral bays. For the columns, I-shaped section with 345 MPa resistivity was used, which were patched at 1.83 m from the first, third, fifth and seventh stories. This patch is designed for simultaneous transfer of axial force and bending anchor. Column connections are modelled as pinned on the ground story. The beams are also of I section which interact with the concrete story slab. The reinforced concrete shear walls have been used around the ground story in order to avoid horizontal displacement of the system (due to joint fittings at the base). The base level is thus moved to the first story. The ground story seismic mass is 965 tons and first, second to eighth and ninth story seismic mass is 1010, 989 and 1070 tons, respectively, so the total mass of the structure is 9,000 tons. Since 9-story SAC9 project building is in regular plan, in this paper, only the two-dimensional representation frame of the north-south peripheral frame is modelled. Half of the seismic mass is assumed to this frame. For modelling, M1 modelling method developed by Gupta and Krawinkler was used [25]. The effect of P-Δ is considered, but the properties of the coupling source are not considered. In M1 model all beams and columns are modelled using the center line method. The main reason for choosing this structural system is that the main impartial of this paper is to evaluate the different types of nonlinear seismic demands due to different methods of pushover and study the adequacy of each to the results of nonlinear time history analysis. So, the selected model should be able to provide an acceptable description of the non-elastic demands distribution reproduced in numerical software with minimal modelling details. Following the simulation of M1 model in OpenSEES, the pushover diagram of Gupta's study along with 2D model developed by the authors is shown in Figure 3. The comparison of the two graphs indicates acceptable accuracy in the modelling phase of this study. The reason for the difference lies in two issues. First, Gupta used the idea of concentrated plastic joint for modelling, while the study used the extensive ductility modelled by the fibre element. Second, in software used by Gupta, P-Δ effect is simulated by a virtual column on which a gravity load is attached to a truss member with significance hardness to the main frame, while in this study the effect of nonlinearity of the geometry is defined by the transfer matrix as a feature of OpenSEES software.

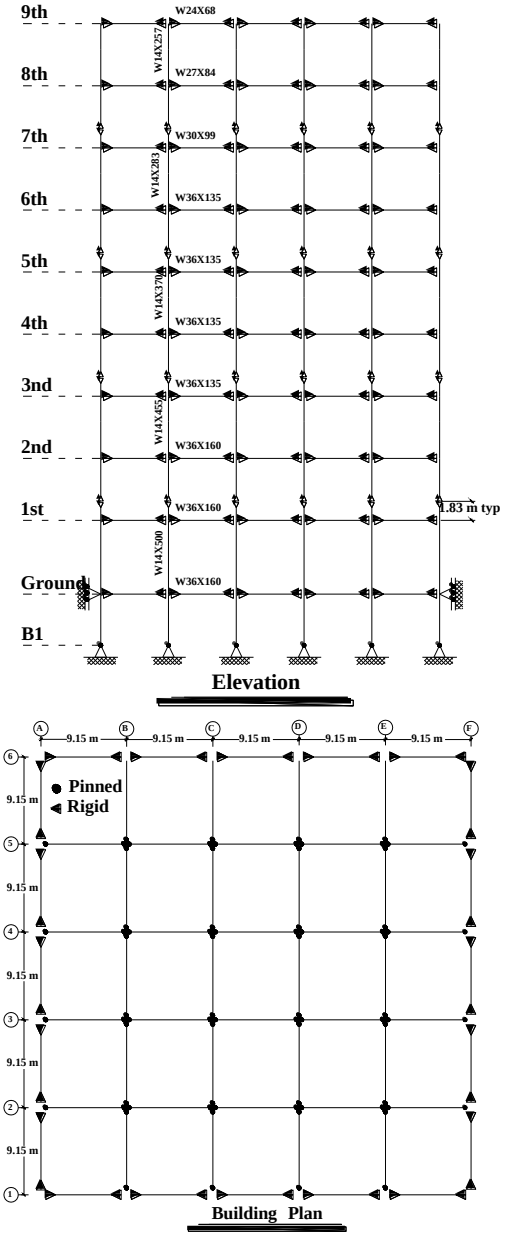

Fig. 2: Elevation and plan of SAC9 structure

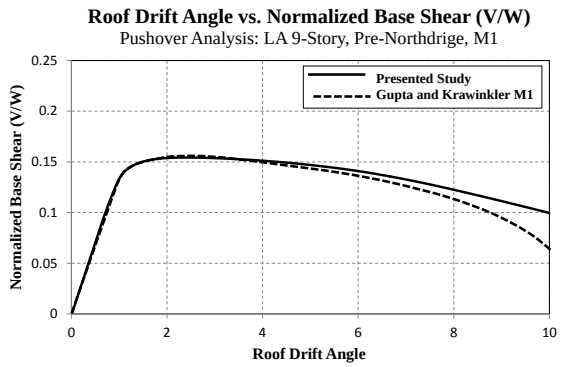

Fig. 3: Comparison of the graph of M1 model pushover in Gupta study with the numerical graph of the present study at 10% overall drift [2]

4. Results

4.1 Seismic input energy of SDOF systems

After introducing far-fault earthquakes in the past three decades, Northridge (1994), Chi Chi in Taiwan (1999) and Kocali (Turkey) earthquakes have shown that many differences are found in near-fault and far-fault earthquakes. So, distinct velocity and acceleration pulses are considered as the most important differences. These pulses, formed due to directivity effects, originate from the kinetic nature of the ground adjacent to the fault plane. The velocity pulses and acceleration pulses' features that contribute to the intrinsic velocity pulse development also play a major role in calculating and determining the absolute and relative input energy of near-fault earthquakes, causing these values to be significantly different from that of far-fault motions.

In far-fault earthquakes, input energy is increased cumulatively and reaches its maximum value at the end of the ground motion. This maximum energy is usually used to create the input energy spectrum. In Figure 4, the first and the second rows are the history of acceleration and velocity of the given earthquake, while the third row represents the elastic reflectance spectrum of input energy in both absolute and relative modes. The fourth row also shows the time-dependent cumulative (relative and absolute) input energy. The depicted graphs are valid for far-fault records of Imperial-Valley (OAK station) (Figure 4b) and Tabas (Ferdows station) earthquakes (Fig. 4a). Also, in order to compare different records, graphs are simply prepared for R = 2 and input energy has been turned to energy equivalent velocity [26] by $V_{EQ}= (2E_{AI}/m)^{0.5}$ and $V_{EQ'}=(2E_{RI}/m)^{0.5}$ for absolute and relative values, respectively. So, it is reasonable to use the energy equivalent velocity to define the size of input energy. As shown in Figure 4a, since there is a high frequency content in acceleration time history for far-fault records, the multiple increase is observed in the velocity time history. These multiple increases cause input energy to grow incrementally and are associated with cumulative damage by multiple nonlinear deformation cycles (low cycle fatigue phenomenon). Therefore, the effective time duration of the earthquake is considered as an important factor for calculating the max far-fault earthquakes' input energy.

On the other hand, near-fault earthquakes have intrinsic long-period velocity pulses that are typically shown in Figure 5a for Northridge (New Hall Station) and Figure 5b for Northridge (Jensen Filter Plant) earthquakes. These two records have the forward directivity effect. This occurs when the propagation velocity of the fault is close to the shear wave velocity. The associated deformation of this shear wave velocity perpendicular to the fault is larger for slip faults. The most important distinction between records with directivity effects is the presence of a distinct pulse in velocity history. Figure 5 shows the energy acceleration, velocity, time history and energy spectrum corresponding to Northridge (New Hall Station) and Northridge (Jensen Filter Plant) earthquakes for R = 2. As shown in Fig. 4, in the velocity record, the bi-directional velocity pulse is a sign of forward directivity motion. This pulse may be due to high-frequency peak acceleration (similar to that found in far-fault earthquakes), which can be referred to Northridge (Jensen Filter Plant) earthquake record. In this record, as shown in Figure 5b, there is a high frequency earthquake with no visible pulse. It can also be seen as a distinct pulse in the acceleration record and velocity history, as shown in Figure 5a. This difference can affect input energy reliant on the relative or absolute definition. Studies show that records with directivity effects with no apparent acceleration pulses have similar (absolute and relative) energy spectra [26]. However, the presence of a visible pulse in the acceleration record causes the difference in the relative and absolute energy values in the short and long periods. In the mid-period, the difference in the two types of energy is insignificant, but in the long-term, the relative energy is normally larger than the absolute energy. Such a conclusion can be seen for different records with directivity effects where a visible pulse is seen in the acceleration record. The assessment of the energy-time history of the two records reveals an additional significant aspect of acceleration pulses. If the acceleration record is pulse-free, the input energy gradually increases over time and reaches its maximum value at the end of the acceleration. While for the record with the pulse is evident in the acceleration, the input energy reaches its maximum value in a very short time with the minimum time required to accumulate energy. In other words, the difference in the absolute and relative input energy over a small period of time increases dramatically. This difference can be justified for two reasons:

• The kinetic energy of the ground does not depend on the response of the structure and the corresponding spectral period (often with positive values).

• The additional work performed by the ground acceleration will be relatively positive to the system response if the ground velocity is in phase with the relative velocity of the structure.

Therefore, when the velocity phase of the ground is not the same as the structure relative velocity, the difference in the two definitions provided for energy results in its minimum. As shown in Figures 5a and 5b, it is clear that for a visible pulse in acceleration, the relative and absolute input energy is different in the low and high periods. On the other hand,

the input energy is usually accompanied by a significant jump. Within this range, the history of the relative and absolute accumulated energy is different. However, if the near-fault earthquake acceleration does not have a large pulse in the acceleration record, despite a visible pulse in the velocity record, relative and absolute spectral energy values are close to one another.

The above observations can be represented as the ratio of absolute to relative input energy for all near-fault records in this paper in the form of basic energy spectra. These two parameters are shown in Figure 6. In this figure, the vertical axis is the ratio of absolute to relative energy and the horizontal axis is the period. These basic spectra are plotted for the three R values of 2, 4 and 6 to observe the effects of nonlinearity on this ratio. The study results of Kalkan (2006) [26], both from the appearance of the resulting graphs and values, are well consistent with the results obtained from samples of acceleration, velocity, and energy equivalent velocity time history for near-fault earthquakes with forward-directivity effect.

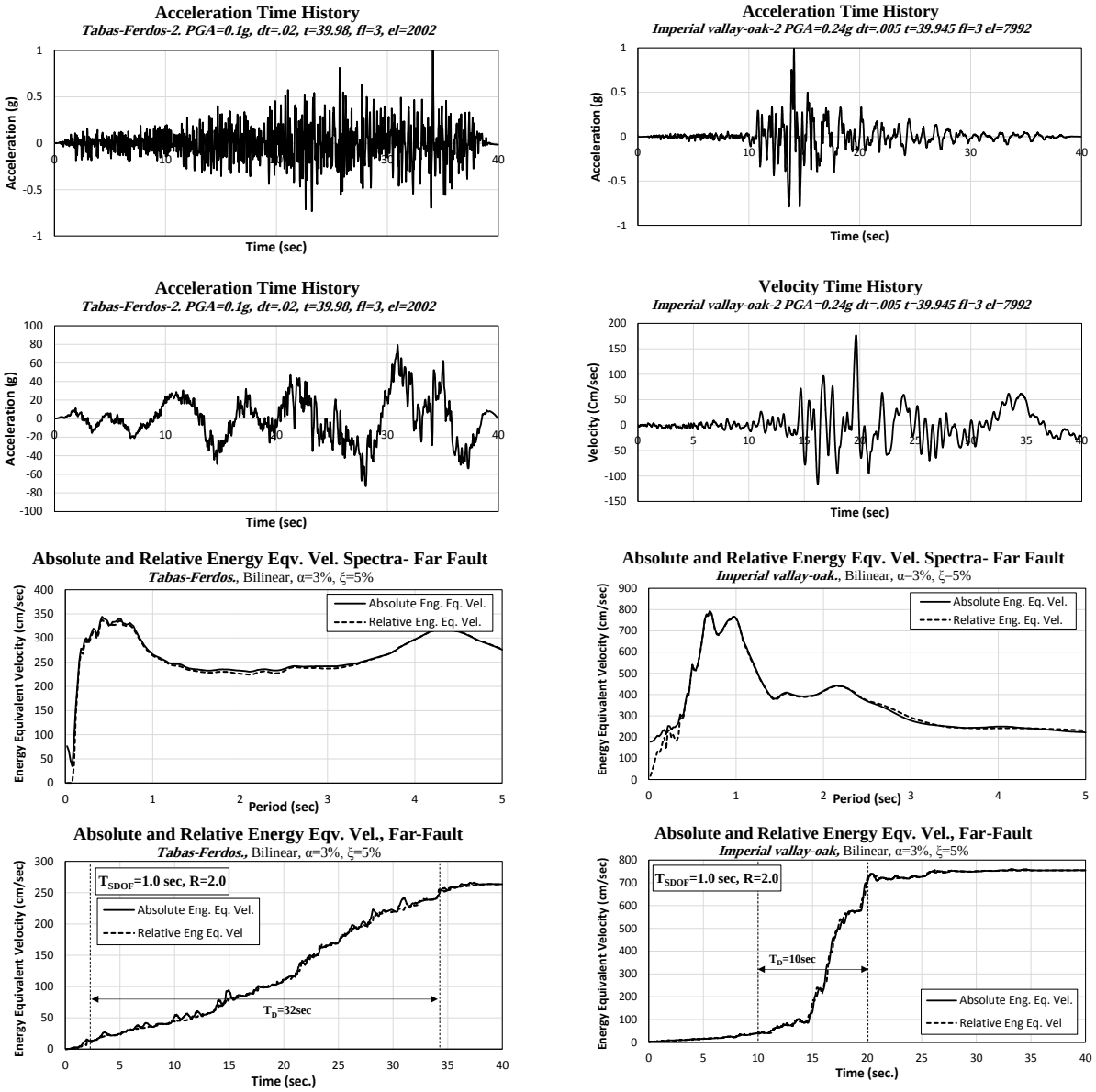

a) Far-fault earthquake with high frequency content b) Far-fault earthquake with limited frequency content

Fig. 4: Time history of acceleration, velocity and energy equivalent velocity, VEQ, along with energy equivalent velocity spectrum for two far-fault earthquakes, R = 2 and T=1.0 Sec

4.2 The relationship between seismic input energy and response of SDOF systems

The most fundamental objective defined in performance-based design is that the seismic design ensures sufficient structural elements ductility and energy dissipation capacity to limit damage to the structure in terms of story drift angle and deformation of members to values corresponding to performance levels. Obviously, the evaluation and realization of this basic principle makes sense in the non-elastic phase. The key point of this topic is to identify the seismic performance of the structure corresponding to the final yield capacity of the members and compare them with the maximum displacement response. Review of various studies show that to provide

this key concept, the use of energy balance formulation is an efficient and effective method for seismic evaluation. This formulation allows a more rational evaluation of the absorbed and dissipated energy mechanism and how it is related to the size of input energy of the structure. For this reason, it seems that introducing appropriate parameters based on energy balance can lead to reliable results in terms of the estimation of maximum demands. In addition, the degree of earthquake-induced damage can also be minimized. The promotion and development of these two basic concepts is gradually becoming a definitive requirement in performance-based design engineering. In recognition of this, various indicators have been developed based on energy balance [7-10]. All the proposed indicators use absolute or relative formulation and the earthquake profile is not considered if it is cyclical nature of far-fault earthquakes or pulse nature of near-fault earthquakes. Far-fault records have a cyclic behaviour, so the structural damage level is independent on maximum deformation. because the continuity of low cycle fatigue also has a significant effect on the structural damage [27-30]. This indicates that the cumulative input energy should depend on a common parameter or index that can effectively define the potential for damage. However, for near-fault earthquakes, much of the structural damage occurs in only a few finite plastic cycles, which is dependent on pulse effects due to the instantaneous energy demand. In this case, the concept of low cycle fatigue is generally unimportant and the cumulative damage is directly related to the maximum structural deformation.

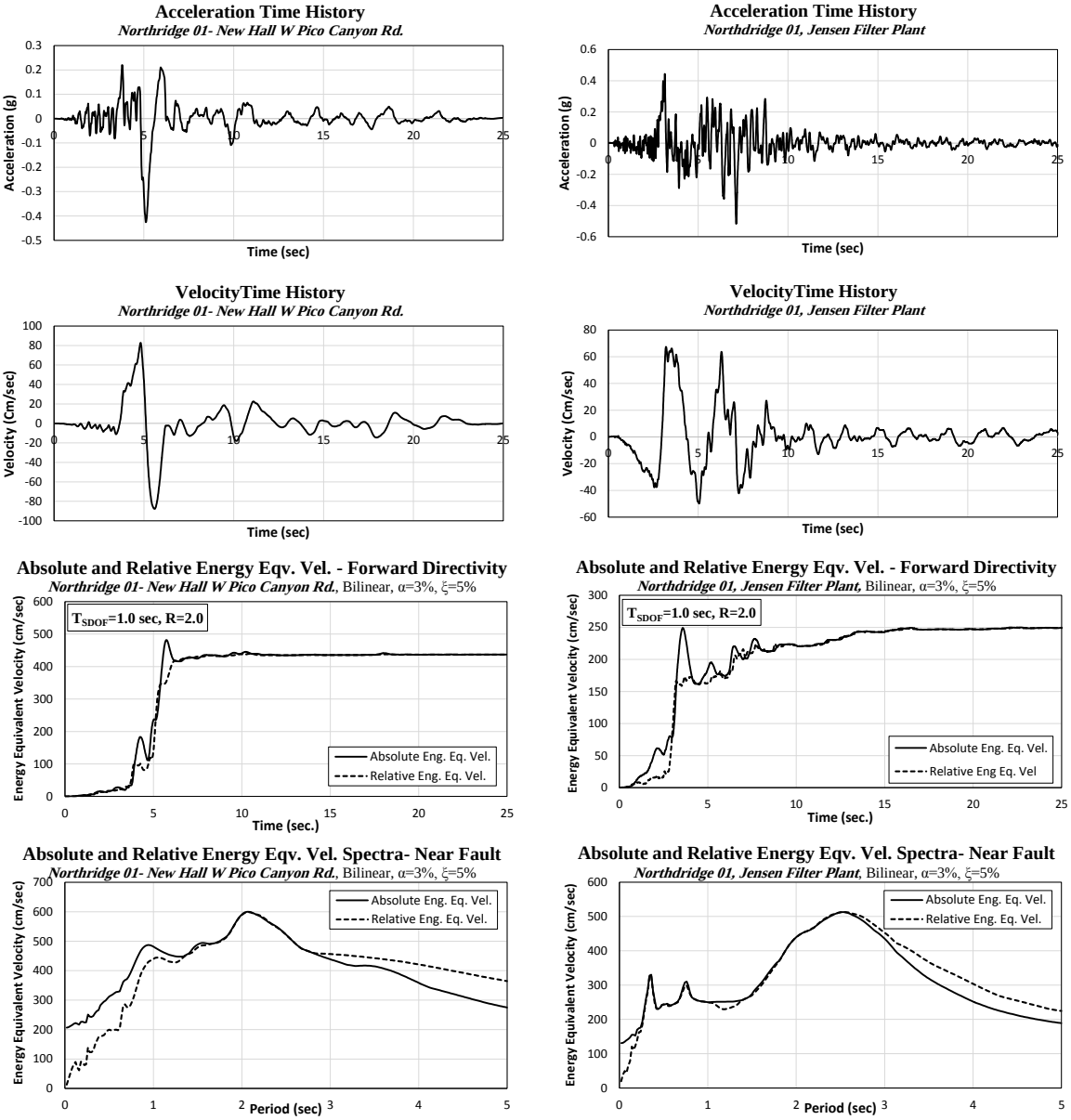

a) with clear pulse in velocity b) no distinct pulse in velocity

Fig. 5: Time history of acceleration, velocity and energy equivalent velocity, VEQ, along with energy equivalent velocity spectrum for two near-fault earthquakes with and without a visible pulse in acceleration record, R = 2 and T=1.0 Sec

On the one hand, using cumulative input energy as the response index may lead to inaccurate results for near-fault earthquakes with a visible pulse in the acceleration record because the maximum energy demand in such a record has a significant peak in the early phases of the response time history of energy causing an effect more serious than the input energy stored at the end of the earthquake record. This remarkable jump in energy may be seen in the history of relative or absolute energy and depends on the ratio of the structural period to the dominant period of the earthquake pulse, so the difference in the time history of earthquake energy and consequently the energy spectrum increases in both relative and absolute modes. In fact, in addition to being important for evaluating the reliability of different response indicators proposed based on relative and absolute energy formulations, and depends on the management of different definitions of earthquake input energy and their dependence on the maximum deformation demands. For this reason, in this section of the paper, the relationship between structural demands and earthquake characteristics is investigated. For this purpose, the definition of maximum Effective Cyclic Energy (ECE), proposed by Kalkan (2006) has been used [26]. This parameter represents the maximum value of energy dissipation during hysteresis and damping loops (the time interval demanded to reverse the system velocity). In order to define the relationship between ECE and maximum structural displacement, a nonlinear time history analysis of SDOF system with T=1 sec. corresponding to R = 2 was used. Fig. 6 shows the energy history equivalent to cumulative velocity, structural velocity, displacement, and hysteresis curve of the nonlinear time history analysis of SDOF system against two far and near-fault earthquakes. Northridge earthquake record (Pico Canyon station) is near-fault type and Imperial Valley (OAK station) is far-fault type. Since the records used in this section were not scaled, R coefficient was obtained by changing the yield strength. In this Fig., the relative input energy formulation used according to Eq. 8:

$$E_{KR} + E_{\xi} + E_s + E_H = E_{RI} \quad (8)$$

where, E_{RI} is relative input energy, E_{KR} is relative kinetic energy, E_I denotes the work done by the inertia force ($m\ddot{u}_t$) affected the structure, which is equivalent to the work done by the total base shear force due to the ground motion. On the other hand, E_{RI} signifies the work done by the structure with a fixed support by equivalent lateral force. In addition, E_{ξ} is the damping energy and E_s is the elastic strain energy. Eq. (8) can be written as Eq. (9):

$$m\frac{\dot{u}}{2} + \int (c\dot{u})du + \int f(u)du = -\int m\left(\ddot{u}_g\right)du = -\int m\ddot{u}_g\,\dot{u}dt \quad (9)$$

The advantage of Figure 7 is that it allows a more accurate evaluation of seismic demands and their relationship to a variety of input energy components. Given that the damage to the components of the structure is directly dependent on the energy dissipation, Figure 7 shows that the kinetic energy is eliminated when reversing the velocity of the structure, thus the sum of the damping and cyclic energy equals the relative input energy. This condition can also be observed based on the dotted points in the force-deformation hysteresis cycle. The energy balance between two points of maximum response can be written as Eq. 10:

$$\Delta E_H + \Delta E_D = \Delta E_{RI} \quad (10)$$

where ΔE_H is the energy established by recoverable strain energy ΔE_s and non- recoverable strain energy, ΔE_P and ΔE_D is the energy created by viscous damping energy. The maximum right side of Eq. 10, $\Delta E_{RI,max}$ can be considered as the effective cyclic energy, ECE. ECE is the work done over a finite time interval that reverses the structural velocity at the beginning and the end. As shown in Figure 7, ECE reaches its maximum value immediately after the maximum deformation of the structure. It should be noted that ECE depends on the dynamic properties of the structure (period, hysteresis law, damping, and ductility), in addition to the earthquake features. Although Eq.s 6 and 10 are calculated on the basis of relative input energy, ECE is not very dependent on the choice of energy definition whether absolute or relative. In addition, Figure 7 shows that for far-fault earthquakes, ECE definition is not feasible, because in this type of earthquake, non-elastic deformations with more cycles are lost, so the structure experiences a greater number of times of yield level. In such a case, the use of total energy dissipation can be used as an appropriate index for understanding the nonlinear behaviour of structures.

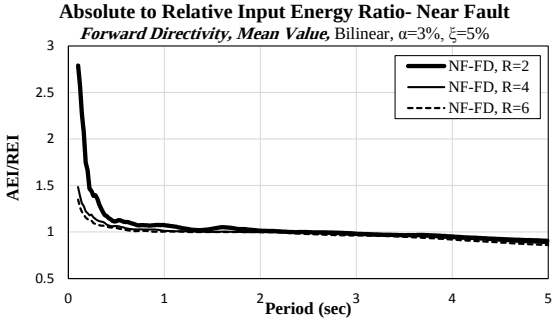

Fig. 6: The changes in the ratio of absolute to relative energy versus period for R = 2, 4, 6 in near-fault earthquakes

4.3 Seismic input energy of MDOF system

The common form of the absolute input energy for SDOF system in Eq. 4 has been generalized and extended by Uang and Bertro (1990) to a multi-degree n-stories system as follows [6]:

$$\frac{1}{2}\{\dot{u}_t\}^T[m]\{\dot{u}_t\} + \int(\{\dot{u}_t\}^T[c])d\{u\} + \int\{f(u)\}^T d\{u\} = \int\left(\sum_{j=1}^{N} m_j\ddot{u}_{t(j)}\right)du_g = \int\left(\sum_{j=1}^{N} m_j\ddot{u}_{t(j)}\right)\dot{u}_g dt \quad (11)$$

In the above Equation, [m] is the matrix of mass, [c] is the matrix of damping and {u} is the relative displacement vector. In addition, m_j is the concentrated mass of the story j, $\ddot{u}_{t(j)}$ is the absolute acceleration recorded in the story j, and N is the number of stories of the structure. The left side of Eq. (11) corresponds to the total work performed by the inertia force ($m_j\ddot{u}_{t(j)}$) on each story as a result of the ground displacement, u_g, at the foundation level. In this way the relative energy of MDOF system can be estimated as follows:

$$\frac{1}{2}\{\dot{u}\}^T[m]\{\dot{u}\} + \int(\{\dot{u}\}[c])d\{u\} + \int\{f(u)\}d\{u\} = \int\left(\sum_{j=1}^{N} m_j\ddot{u}_g\right)d\{u\} = \int\left(\sum_{j=1}^{N} m_j\ddot{u}_g\dot{u}_{(j)}\right)dt \quad (12)$$

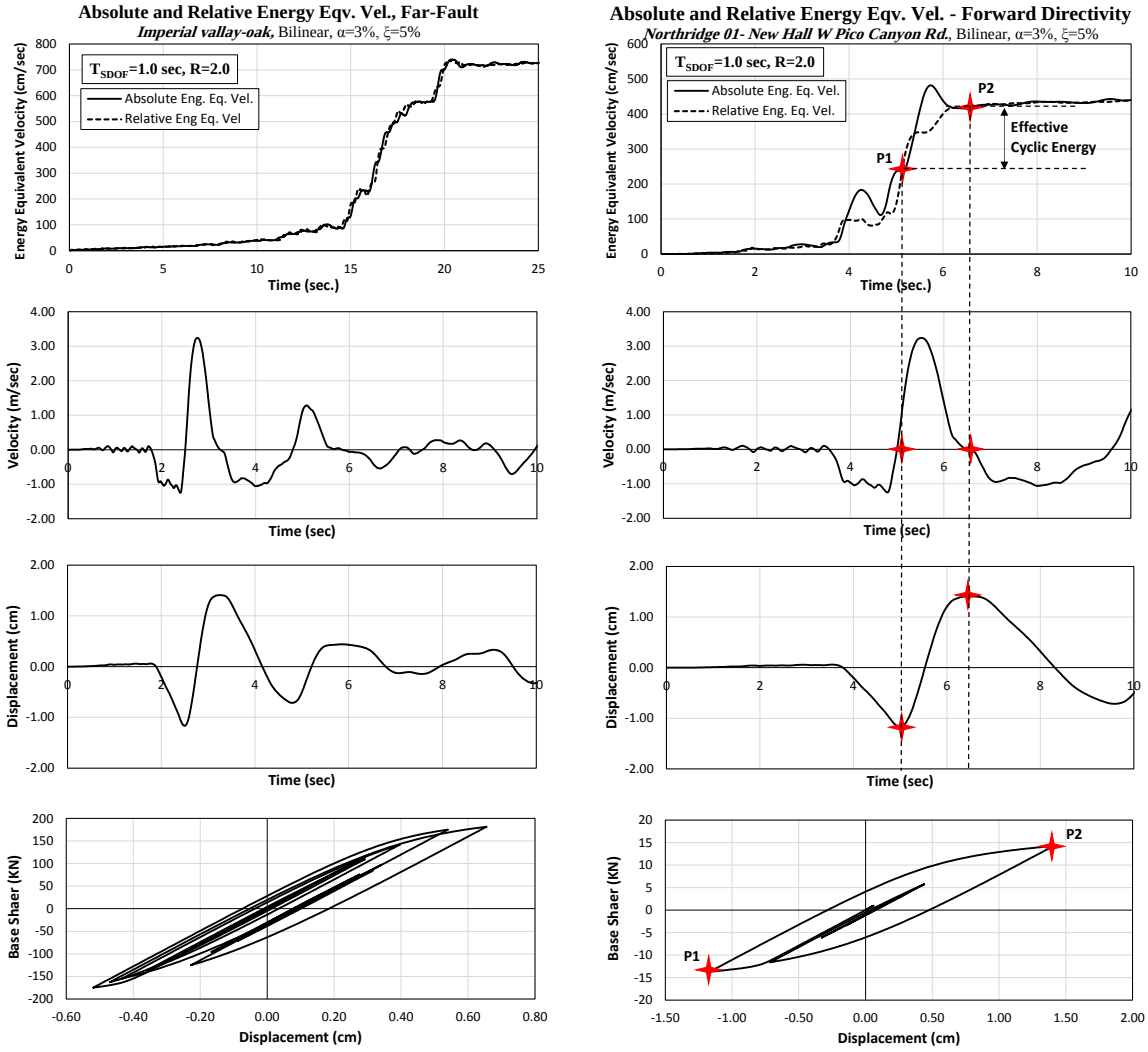

a) Far-fault earthquake b) Near-fault earthquake

Fig. 7: The relationship between effective cyclic energy, ECE and displacement, velocity and hysteric demands of SDOF system with R = 2 and T = 1.0 sec in two near-fault and far-fault modes.

The difference in the relative and absolute energy formulation (Eq.s 11 and 12) can be written on the basis of the difference in kinetic energy formulation as suggested by Kalkan (2006) [26]:

$$E_{AI} - E_{RI} = \frac{1}{2} m\dot{u}_g^2 + \sum_{j=1}^{N} m\dot{u}_g \dot{u}_{(j)} \quad (13)$$

4.4 The input energy and effect of near fault earthquakes in MDOF system

In this part, the relationship between the near-fault earthquake effect and input energy content is evaluated by examining FRN15B3 frame response. The given model is analysed against two near-fault records with forward directivity effects. The two records were carefully selected, one of which had a visible pulse in the acceleration history and the other had no pulse, but both records had a visible pulse in their velocity history, which attempted to minimize the relationship between input energy and seismic demands. The two selected records are related to Northridge (New Hall Station) and Landers (Yermo Fire Station) earthquakes, which are provided by SN3 and SN8, respectively. Figures 8 and 9 show the relative and absolute cumulative input energy history, respectively, with kinetic energy at 4 different levels of nonlinear behaviour (R = 1.0, 2.0, 4.0, and 6.0), the former corresponding to SN3 record and the latter to SN8 record. It should be noted that for SN3, there is a visible pulse, whereas in SN8 record, this pulse is only present in the velocity record. The reason for choosing FRN15B3 model is that it is one of the most common midrange structures in Iran and therefore the higher mode and degree of freedom effects would be apparent. In addition, Figure 10 shows the maximum inter-story drift for different values of R. The evaluation of Figure 10 shows that for R = 2, if there is a visible pulse in the earthquake acceleration history (similar to SN3 record), the maximum demand for story drift occurs mainly in the upper stories. Another point is that for SN3 record, the increase in R reduced the effect of higher modes and the major response was in the lower stories due to inelastic instability. This is justified by the maximum accumulation of IDR in the lower stories of the structure. Of course, how close the pulse period is to the second mode period, can be a key factor in the influence of the drift distribution over the height under the effect of higher modes. However, for R = 2 the results of SN8 record (where the cumulative input energy is gradually increasing) show that in addition

to the activation of the higher modes effect on the upper stories, the drift demands in the lower stories of the structure are also significant. With increasing R corresponding to SN8 results, the maximum demands accumulate in the lower stories and somehow the effect of the inelastic instability overcomes the final response of the structure. The obtained results in this section are in good agreement with the study results conducted by Uang and Bertero (1990) [6] and Kalkan (2006) [26]. Figures 8 and 9 show the comparison of the relative and absolute input energy of SN8 and SN3 records where the input energy level in SN8 record is much larger than SN3. However, for low R, IDR_{max} of both records is the same. In order to justify this, it can be said that in SN3 record a significant quantity of earthquake input energy enters the structure in a short period of time (approximately 2 seconds). Therefore, the structure will not have enough time to react to this accumulated energy level; therefore, the greater the earthquake input energy, the greater the imposed demands on the structure. In addition, the highest amount of IDR_{max} is precisely dependent on the cumulative input energy. The higher the cumulative input energy, the greater the demands over the structure height.

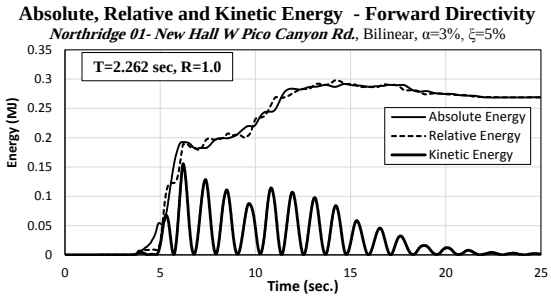

(a) R=1.0

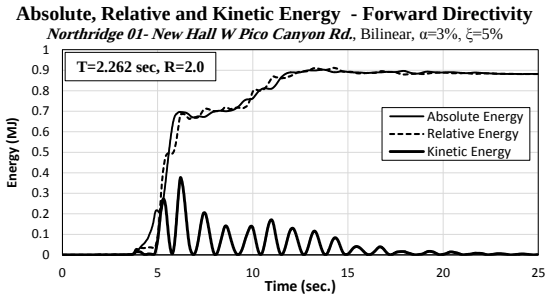

(b) R=2.0

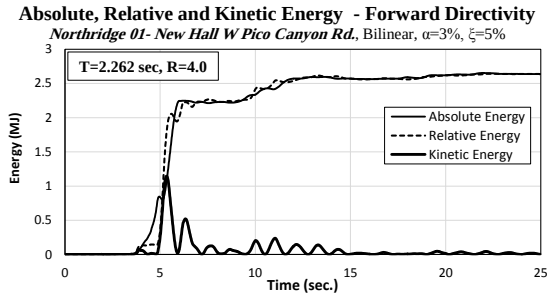

(a) R=4.0

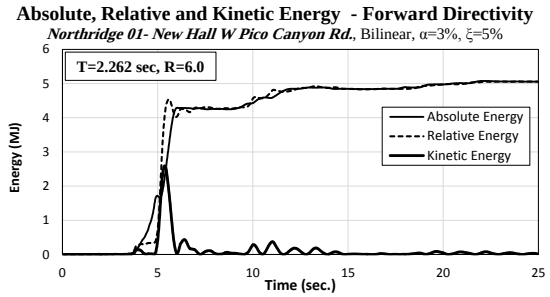

(b) R=6.0

Fig. 8: The relative, absolute, and kinetic input energy history due to Northdridge-New Hall (SN3) earthquake for R = 1, 2, 4, 6 and FRN15B3 (T = 2.262 Sec.)

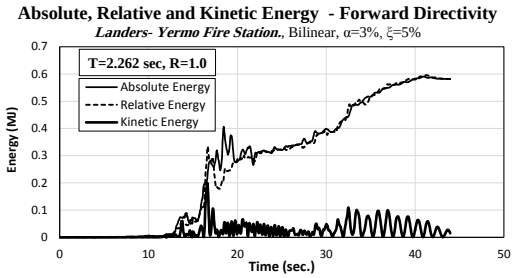

(a) R=1.0

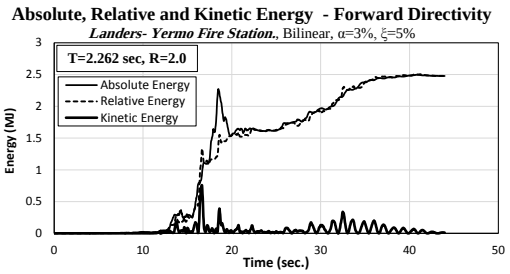

(b) R=2.0

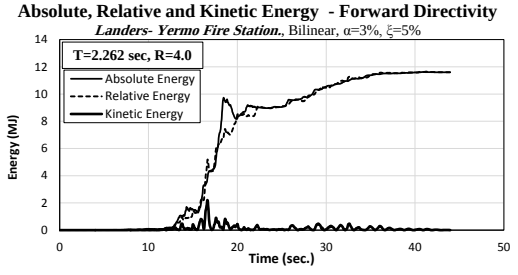

(c) R=4.0

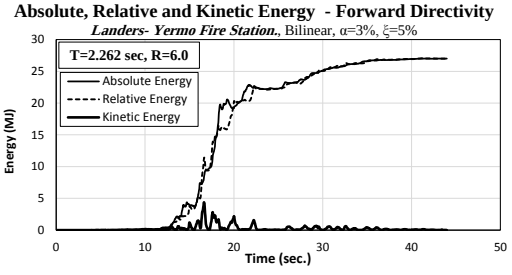

(d) R=6.0

Fig. 9: The relative, absolute and kinetic input energy history due to Landers-Yermo (SN8) earthquake for R = 1, 2, 4, 6 and FRN15B3 (T = 2.262 Sec.)

5. Conclusion

For several years, various researchers have attempted to develop performance-based design concepts using energy principles. The most important point they have considered is to calculate the target displacement of a structure under the pushover analysis by means of energy definition. Perhaps what distinguishes studies related to this topic is the type of energy that is taken into account. One of the most common methods of calculating energy-based target displacement is the use of structural input energy, which is defined in two relative and absolute forms. Of course, the use of cyclic energy dissipated by the equivalent SDOF system can also be considered. It should be noted that the presence of a pulse in the near-fault earthquake causes different input energy demand and consequently the distribution of energy demand is lost due to cyclic and damping behaviour along with the kinetic and elastic strain energy in comparison with the far-fault earthquake. This paper, attempted to evaluate the effect of pulse-type near-fault earthquakes on the inelastic demands of SDOF and MDOF steel moment. In this regard, first, the relationship between Effective Cyclic Energy, ECE and displacement responses, velocity and hysteretic curves of SDOF systems in two near and far fault earthquakes were investigated. Then, by examining the relative and absolute cumulative input energy history along with the kinetic energy in one section and the maximum inter-story drift for 4 different levels of nonlinear behaviour (R = 1.0, 2.0, 4.0, and 6.0) in the other section, the effect of higher modes was evaluated. The results are given below.

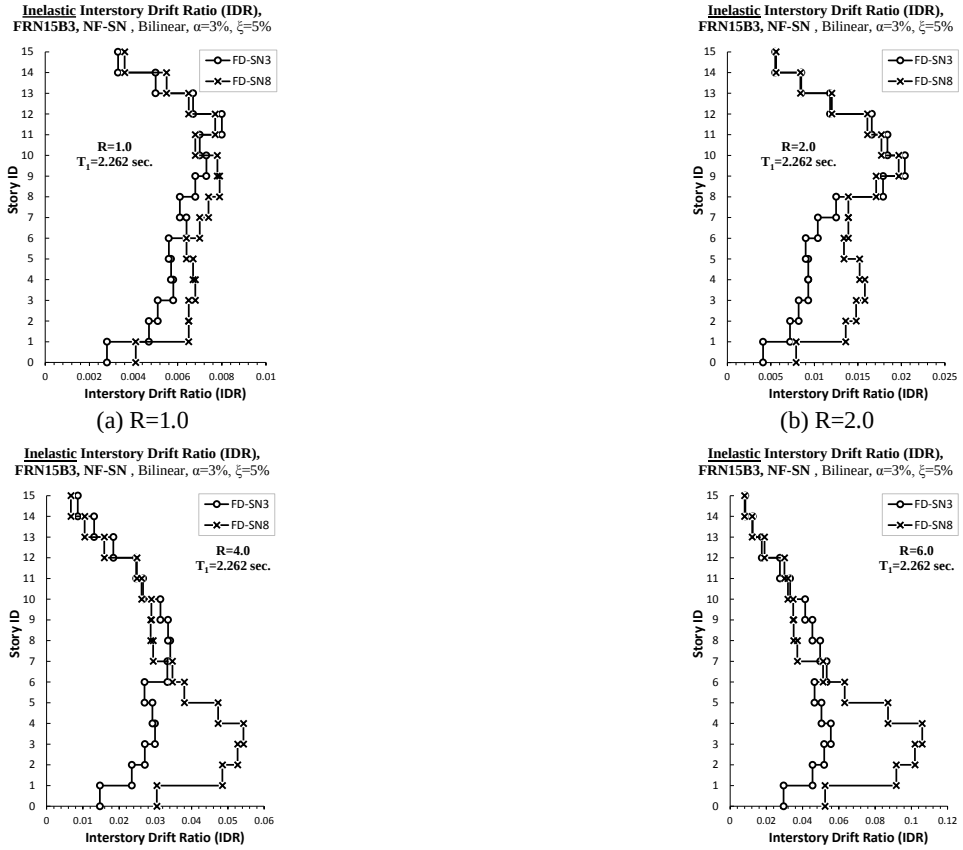

(a) R=1.0 (b) R=2.0

(c) R=4.0 (d) R=6.0

Fig. 10: The maximum distribution of inter-story drift ratio at altitude due to SN3 and SN8 earthquakes for R = 1, 2, 4, 6 and FRN15B3 (T = 2.262 Sec.)

1. For far-fault records due to cumulative damage by multiple nonlinear deformation cycles (low cycle fatigue phenomenon), the duration of strong ground motion is an important and key factor to calculate maximum input energy. The frequency content has a significant effect on the velocity-time history and therefore on the value of cumulative damages.
2. There is distinguishing differences between the absolute and relative input energy resulted from records with and without a distinguishable pulse in the acceleration time history. If the record has no pulse in its acceleration, the relative and absolute energy are almost the same in all ranges of the period. The difference increases in a short and long period section if there is a distinguishable acceleration pulse. In the mid-period, the difference is noticeable for both absolute and relative energy, but in the long periods, the relative energy is commonly higher than the absolute energy.
3. For a record without a distinguishable acceleration pulse, the input energy gradually increases over time and reaches its maximum value at the end of the acceleration. Oppositely, for a record without ~~is~~ a distinguishable acceleration pulse, the maximum input energy cumulated

shortly and, the difference in the absolute and relative input energy over a short period increased dramatically.

4. For far fault ground motions, the low fatigue cycle is an important factor and causes structural damages. The importance of this factor is almost greater than the maximum inelastic deformations, where a few finite plastic cycles happen under near-fault earthquakes. Therefore, in this case, the cumulative damage is related to the maximum structural deformation instead of the low fatigue cycle phenomenon.

5. In the near-fault ground motions, the peak energy demand occurs in the early phases of cumulative energy time history. This phenomenon becomes more crucial when there is a distinguishable acceleration pulse. Therefore, a remarkable jump in energy might be seen in the relative or absolute energy time history and it depends on the ratio of structure period to the earthquake's predominant pulse period. Hence, cumulative input energy as the response index may lead to inaccurate results for these types of records.

6. The maximum inter-story drift profile is a function of inelastic level and the type of near-fault motions. For instance, for the record without distinguishable acceleration pulse (SN3) and lower values of R, the peak IDRs is located at the upper stories due to the contribution of higher modes. Whereas for a record with a distinguishable acceleration pulse and the same value of R, the peak IDRs is located at the lower stories. This peak cumulative value increases while the R-value increases for both with and without a distinguishable acceleration pulse. But the intensification for a distinguishable acceleration pulse record (SN8) is more significant.

7. In the assessment of inelastic behavior of the structure under near-fault ground motions, the effective time of the cumulative input energy is a more important factor than the value of maximum input energy. This factor becomes meaningful while the acceleration has a distinguishable pulse both in velocity and acceleration time history. In interpreting this phenomenon, it can be stated that a significant part of earthquake input energy enters the structure in a short duration and therefore, the structure will not have enough time to respond to this accumulated energy level.

References

[1] Housner, G. W. (1956). *Limit design of structures to resist earthquakes*, Paper presented at the Proc. of 1st WCEE, Berkeley, California.

[2] Park, Y.-J., Ang, A.-S., and Wen, Y.-K. (1984). *Seismic Damage Analysis and Damage-Limiting Design of RC Buildings*, University of Illinois Engineering Experiment Station. College of Engineering. University of Illinois at Urbana-Champaign.

[3] Krawinkler, H. (1987). Performance assessment of steel components. *Earthquake spectra*, Volume 3, No. 1, 14 Pages.

[4] Tembulkar, J. M. and Nau, J. M. (1987). Inelastic modeling and seismic energy dissipation. *Journal of Structural Engineering*, Volume 113, No. 6, 14 Pages.

[5] Minami, T. and Osawa, Y. (1988). Elastic-plastic response spectra for different hysteretic rules. *Earthquake engineering & structural dynamics*, Volume 16, No. 4, 13 Pages.

[6] Uang, C. M. and Bertero, V. V. (1990). Evaluation of seismic energy in structures. *Earthquake engineering & structural dynamics*, Volume 19, No. 1, 13 Pages.

[7] Decanini, L. D. and Mollaioli, F. (2001). An energy-based methodology for the assessment of seismic demand. *Soil Dynamics and Earthquake Engineering*, Volume 21, No. 2, 22 Pages.

[8] Chou, C. C. and Uang, C. M. (2000). Establishing absorbed energy spectra-an attenuation approach. *Earthquake engineering & structural dynamics*, Volume 29, No. 10, 14 Pages.

[9] Chai, Y. and Fajfar, P. (2000). A procedure for estimating input energy spectra for seismic design. *Journal of Earthquake Engineering*, Volume 4, No. 4, 22 Pages.

[10] Riddell, R. and J. E. Garcia (2001). Hysteretic energy spectrum and damage control. *Earthquake engineering & structural dynamics*, Volume 30, No. 12, 25 Pages.

[11] Leelataviwat, S., Goel, S. C., and Stojadinovic, B. (2002). Energy-based seismic design of structures using yield mechanism and target drift. *Journal of Structural Engineering*, Volume 128, No. 8, 8 Pages.

[12] Chou, C. C. and Uang, C. M. (2003). A procedure for evaluating seismic energy demand of framed structures. *Earthquake engineering & structural dynamics*, Volume 32, No. 2, 15 Pages.

[13] Kalkan, E. and Kunnath, S. K. (2006). Effects of fling step and forward directivity on seismic response of buildings. *Earthquake Spectra*, Volume 25, No. 2, 23 Pages.

[14] Kamali-Firozabadi, S.J. (2011). *Using energy method to estimate the required displacement of steel moment frames*. Master of Science Thesis. Khaje Nasir Toosi University of Technology, Department of Civil Engineering. (In Persian)

[15] Vahdani, R. and Gerami, M. and Vaseghinia, A. (2017). Structural damping and displacement ductility effects on input energy spectrum of earthquake. *Journal of Structural and Construction Engineering (JSCE)*, Volume 5, Issue 2, 17 Pages. (In Persian)

[16] Fang, C., Zhong, O., Wang, W., Hu, Sh. and Qiu, Q. (2018). Peak and residual responses of steel moment-resisting and braced frames under pulse-like near-fault earthquakes. *Engineering Structures*, Volume ١٧٧, 19 Pages.

[17] Xin, L., Li, X., Zhang, Z. and Zhao, L. (2019). Seismic behavior of long-span concrete-filled steel tubular arch bridge subjected to near-fault fling-step motions. *Engineering Structures*, Volume 180, 12 Pages.

[18] Bertero, V. V., Herrera, R., and Mahin, S. (1976). *Establishment of design earthquakes-evaluation of present methods*, Paper presented at the International Symposium on Earthquake Structural Engineering, St. Louis, 1, 29 Pages.

[19] Iranian Building Codes and Standards, Iranian Code of Practice for Seismic Resistant Design of Buildings, 4th Edition, BHRC-PN S-253, Road, Housing and Urban Development Research Center, Iran, 2014.

[20] Computers and Structures, Inc., Etabs 2016—extended 3D analysis of building systems, nonlinear, Berkeley, California 94704, USA.

[21] ANSI/AISC 360-10 (2010). Specification for Structural Steel Buildings. American Institute of Steel Construction, One East Wacker Drive, Suite 700, Chicago, Illinois 60601-1802 of Civil Engineers.

[22] McKenna, F. (2011). "OpenSEES: a framework for earthquake engineering simulation", Computing in Science & Engineering, 13(4), pp. 58-66, 2011. https://doi.org/10.1109/MCSE.2011.66

[23] Baker, J. (2007). Quantitative classification of near-field ground motion using wavelet analysis. *Bulletin of the Seismological Society of America*, Volume 97, No. 5, 15 Pages.
[24] Kramer, S.L. (1996). Geotechnical Earthquake Engineering. Prentice Hall, New Jersey, 1996.
[25] Gupta, A. and Krawinkler, H. (1999). Seismic demands for the performance evaluation of steel moment resisting frame structures, Stanford University.
[26] Kalkan, E. (2006). *Prediction of Seismic Demands in Building Structures*, Ph.D. Thesis. University of California Davis.
[27] Fajfar, P. and Vidic, T. (1994). Consistent inelastic design spectra: hysteretic and input energy. *Earthquake engineering & structural dynamics*, Volume 23, No. 5, 14 Pages.
[28] Kunnath, S. and Chai, Y. (2004). Cumulative damage-based inelastic cyclic demand spectrum. *Earthquake engineering & structural dynamics*, Volume 33, No. 4, 21 Pages.
[29] Sucuoğlu, H., Yücemen, S., Gezer, A., and Erberik, A. (1998). Statistical evaluation of the damage potential of earthquake ground motions. *Structural Safety*, Volume 20, No. 4, 21 Pages.
[30] Teran-Gilmore, A., and Jirsa, J. O. (2005). A damage model for practical seismic design that accounts for low cycle fatigue. *Earthquake spectra*, Volume 21, No. 3, 29 Pages.